[7] U. Witt, R.-J. Müller, W.-D. Deckwer, *J. Environ. Polym. Degrad.* **1997**, *5*, 81 – 89.
[8] E. Rantze, I. Kleeberg, U. Witt, R.-J. Müller, W.-D. Deckwer, *Macromol. Symp.* **1998**, *130*, 319 – 326.
[9] U. Witt, R.-J. Müller, W.-D. Deckwer, *J. Environ. Polym. Degrad.* **1995**, *3*, 215 – 223.
[10] J. C. G. Ottow, *Naturwissenschaften* **1978**, *65*, 413 – 423.
[11] U. Seeliger (BASF AG), Press release, Ecoflex®—Biologisch abbaubarer Kunststoff von BASF, **1998**.
[12] J. M. G. Cowie, *Chemie und Physik der Polymeren*, VCH, Weinheim, **1976**, p. 96.
[13] I. Kleeberg, C. Hetz, R. M. Kroppenstedt, R.-J. Müller, W.-D. Deckwer, *Appl. Environ. Microbiol.* **1998**, *64*, 1731 – 1735.

Radical Dimerization of 5,5′-Diphenyl-3,3′,4,4′-tetramethoxy-2,2′-bipyrrole: π Dimer in the Crystal, σ Dimer in Solution.**

Andreas Merz*, Jürgen Kronberger, Lothar Dunsch, Andreas Neudeck, Andreas Petr, and Laszlo Parkanyi

Dedicated to Professor Gottfried Märkl on the occasion of his 70th birthday

The highly electron-rich dimethoxypyrrole[1] (DMOP) can be electrochemically polymerized to give good conducting films with conductivities that exceed those of all other 3-, 3, 4-, or *N*-substituted pyrroles, and often even of polypyrrole itself.[2] According to ESR and spectroelectrochemical studies the conductivity of poly-DMOP might involve a transport of the charge carriers not only along the polymer chain but also across neighboring chains by "interchain hopping", similar to the situation in crystalline TTF derivatives and salts of arene cations where π stapling occurs.[3]

Spectroelectrochemical experiments with end-capped pyrrole,[4] thiophene,[5, 6] or mixed thiophene – pyrrole[7] oligomers provide evidence for equilibria between the corresponding radical cations and spinless π dimers. On the other hand a detailed investigation of certain diphenyl polyenes by cyclic voltammetry suggested that the corresponding radical cations dimerize to σ dimers and not to π dimers.[8] In the cited work[8] the existence of π dimers of pyrrole and thiophene oligomers was questioned. Recently, the radical cation of ω,ω-diphenyl-α-terthiophene was shown by an X-ray structure to form endless π staples in which π dimers with shorter distances can be recognized.[9] We now report on diphenyltetramethoxypyrrole **1** whose radical cation crystallizes as a spinless π dimer $(\mathbf{1}^{\bullet+} \cdot PF_6)_2$ but dimerizes as a σ dimer in solution at low temperature.

The bipyrrole **1** is obtained as shown in Scheme 1 from easily accessible pyrrole **3**.[1c] The important steps are the partial hydrolysis of the of the ester **2**[10] and the iododecarboxylation of carboxylic acids **3** and **6**.[11] The introduction of

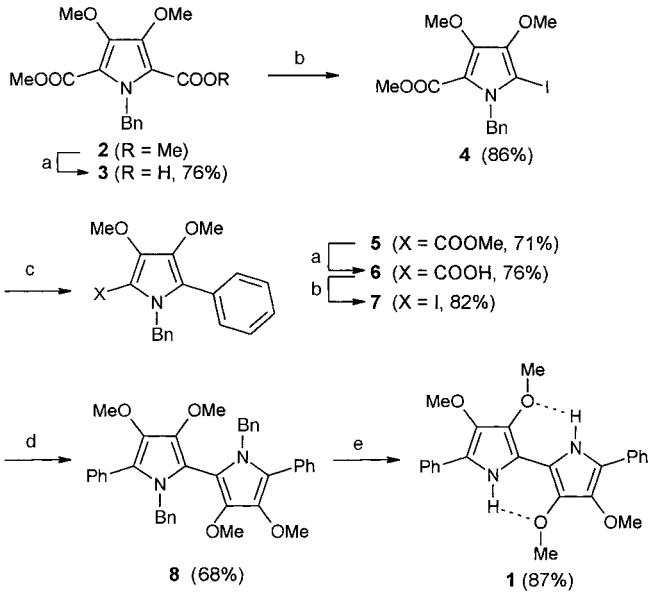

Scheme 1. a) *t*BuOK/H_2O (1/1), THF, 0 °C, 12 h; b) I_2/KI, Na_2CO_3, 12 h, RT, extraction with Et_2O; c) $PhB(OH)_2$, $Pd[PPh_3]_4$, 1,2-dimethoxyethane; d) Cu powder, melt, 200 °C; e) 1. Na, liquid NH_3, 2. EtOH.

the phenyl end group is achieved by a Suzuki coupling[12] and an Ullmann coupling in the melt to give **8**.[13] The benzyl group is an ideal protective group for the pyrrole nitrogen atom because a twist in the bond between the pyrrole units makes the intermediates less prone towards oxidation. The removal of the benzyl groups in **8** is achieved smoothly with Na in liquid NH_3 and quenching with aqueous $NaHCO_3$.[14] Using analogous steps higher oligopyrrole homologues with or without end caps are obtained from **2**.[15]

The bipyrrole **1** crystallizes from a solution in CH_3OH in two different polymorphic crystals. At 90 °C the tetragonal needles **1a** turn, without melting, into the monoclinic cuboids of **1b**, which melt at 171 – 172 °C. Both crystal structures (Figure 1)[16] are dominated characteristically by hydrogen bonds between the NH protons of the pyrrole rings and the oxygen atoms of the inner methoxy groups. In **1b** the almost planar D_{2h} molecules are stabilized in an *anti* conformation of the pyrrole rings by H bonds. In the tetragonal modification **1a** the *syn* oriented bipyrroles are arranged with a 90° turn along a C_2 axes by intermolecular H bonds. The H bonds are also seen in the ^{1}H NMR spectra of **1** as a broad singlet at $\delta =$ 8 ($\delta = 7$ for the corresponding signal in DMOP[1ac]).

[*] Prof. Dr. A. Merz, Dipl.-Chem. J. Kronberger
Institut für Organische Chemie der Universität
D-93040 Regensburg (Germany)
Fax: (+49) 941-943-4121
E-mail: andreas.merz@chemie.uni-regensburg.de
Priv.-Doz. Dr. L. Dunsch, Dr. A. Neudeck, Dr. A. Petr
!Institut für Festkörper- und Werkstofforschung
Helmholtzstrasse 20, D-01069 Dresden (Germany)
E-mail: l.dunsch@ifw-dresden.de
Dr. L. Parkanyi
Chemical Research Center, Hungarian Academy of Sciences
P.O. Box 17, H-1525 Budapest (Hungary)
E-mail: parka@cric.chemres.hu

[**] This work was supported by the Deutsche Forschungsgemeinschaft and the Fonds der Chemischen Industrie.

Supporting information for this article is available on the WWW under http://www.wiley-vch.de/home/angewandte/ or from the author.

  1433-7851/99/3810-1442 $ 17.50+.50/0

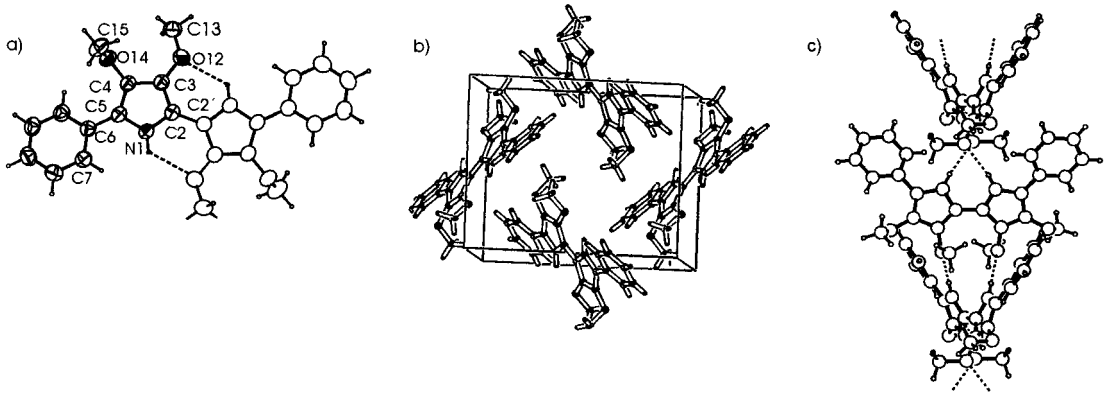

Figure 1. Structures of **1a** and **1b** in the crystal. a) Molecule of the monoclinic modification **1b**. b) Arrangement of **1b** in the unit cell. c) Arrangement of the molecules of the tetragonal modification **1a** along the crystallographic C_2 axis. For bonding parameters see Table 1.

The first redox potential of **1** is only $+0.11$ V (versus Ag/AgCl), hence **1** is easily oxidized to the radical cation $\mathbf{1}^{\bullet+}$ by ferrocinium hexafluorophosphate ($E = +0.49$ V) in CH_3CN. Bluish black, electrically nonconducting needles crystallize from the green solution at $-20\,^{\circ}C$, and an X-ray structure analysis of the crystals was resolved.[16] The crystal (Figure 2)

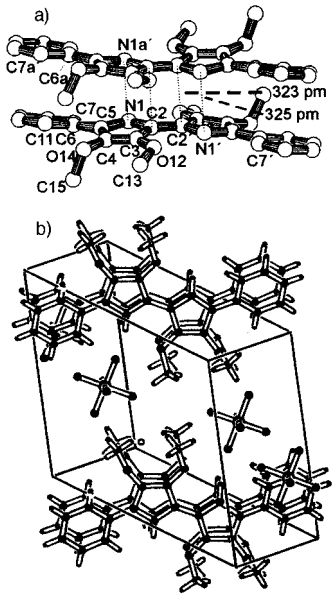

Figure 2. Structure of the π dimer $(\mathbf{1}^{\bullet+} \cdot PF_6)_2$ in the crystal. a) View of the centrosymmetric π sandwich. b) Position of the π-dimeric units in the lattice. For bonding parameters see Table 1.

contains narrowly spaced, sandwich-type centric π dimers $(\mathbf{1}^{\bullet+} \cdot PF_6^-)_2$. Contrary to many π-staple crystals of radical cations of aromatic compounds[3, 17] or tetrafulvalenes,[3, 18] which undergo substoichiometric oxidation to their cations, the two radical cations in $(\mathbf{1}^{\bullet+} \cdot PF_6^-)_2$ are ordered in an almost congruent manner and only slightly laterally displaced. Such an arrangement has been postulated for some π dimers in solution.[19–21] In the above mentioned terthiophene radical cation[9] one of the molecules is rotated by 180° around its longer axis.

The closest contact of the two radical cations in $(\mathbf{1}^{\bullet+} \cdot PF_6^-)_2$ is found at the central bipyrrole bond with C2–C2′ = 323, N1–N1′ = 326, and a central distance of the five membered rings of 344 pm, which corresponds approximately to a van der Waals contact.[22] The structure is widened towards the phenyl groups beginning with atoms C2 and C3 of the pyrrole ring (average distance 376 pm, shortest distance 364 pm). As in **1b**, the inner methoxy groups are coplanar with the corresponding pyrrole ring, as a consequence of hydrogen bond formation, but the outer methoxy groups are rotated out of the plane and in the same direction in both molecules of the π dimer. This is clearly the reason for the deviation from planarity in the outer region of the complex. In a detailed comparison of the structural parameters of **1a**, **1b**, and $(\mathbf{1}^{\bullet+} \cdot PF_6^-)_2$ (see Table 1) the pyrrole rings of **1a** and **1b** have ordinary pyrrole rings, while in the noncongruent halves of the π dimer the distinctly longer bond distance of C2–C3 (ca. 30 pm) and C4–C5 (ca. 50 pm) as well as the shorter bonds of C3–C4 (ca. 30 pm) and C2–C2′ (ca. 60 pm) are remarkable. The dihedral angle N-C2-C2′-N′ in **1b** is exactly 180°, while in the dimer this angle is 178.7° and the C3–C2 and C2′–C3′ bonds are considerably twisted. The C3 methoxy groups in **1a** and **1b** are coplanar with the C3–C4 bond, while in the dimer a dihedral angle of 10° is observed.

The crystals of $(\mathbf{1}^{\bullet+} \cdot PF_6^-)_2$ are diamagnetic. In the solid state only about one thousandth of the expected ESR value for a paramagnetic ESR species is measured, thus, the dimer is not simply a tight package of radical cations. When ether is added to the green CH_3CN solution a fine black precipitate is obtained, which has a much higher paramagnetism (75 % of the theoretical value). This result suggests the presence of radical ions $\mathbf{1}^{\bullet+}$ in an amorphous structure. To clarify if the π dimer $(\mathbf{1}^{\bullet+} \cdot PF_6^-)_2$ is also present in solution UV/Vis and ^1H NMR investigations were undertaken and completed by cyclovoltammetric studies with synchronous measurements of UV/Vis and ESR spectra.

The UV/Vis spectrum of $(\mathbf{1}^{\bullet+} \cdot PF_6^-)_2$ in dry CH_2Cl_2 (2×10^{-5} M under Ar) shows a long-wave band at 739 nm at room temperature as expected for a radical cation, as well as an intense band at 463 nm and a shoulder at 389 nm. Upon cooling the solution down to 173 K a new band at 430 nm reversibly rises on account of the 463 and 739 nm bands with

  1433-7851/99/3810-1443 $ 17.50+.50/0

Table 1. Selected bond lenghts [pm], bond angles [°], and dihedral angles [°].

Bond length:[a]	N–C2	C2–C3	C3–C4	C4–C5	N–C5	C2–C2′
1a	137	139	141	138	138	144
1b	138	138	142	138	138	145
$(\mathbf{1}\cdot PF_6)_2$	137	141	139	143	136	139
$(\mathbf{1}\cdot PF_6)_2$[b]	137	142	138	141	137	139
Bonding angle:	C2-N-C5	N-C2-C3	C2-C3-C4	C3-C4-C5	C4-C5-N	C3-C2-C2′
1a	111.0	106.7	107.9	108.2	106.2	131.1
1b	110.6	107.3	107.4	108.2	106.5	130.5
$(\mathbf{1}\cdot PF_6)_2$	110.3	106.7	107.7	107.5	107.8	128.1
$(\mathbf{1}\cdot PF_6)_2$[b]	110.7	106.4	107.8	108.3	106.8	129.1
Dihedral angle:	N-C2-C2′-N′	C3-C2-C2-C3	N-C5-C6-C11	C4-C5-C6-C7	C4-C3-O14-O15	C3-C4-O12-O13
1a	40.2	45.44	16.5	16.6	1.3	104.63
1b	180.0	180.0	18.8	23.5	0.9	86.1
$(\mathbf{1}\cdot PF_6)_2$	178.7	164.1	20.0	22.0	9.9	99.9
$(\mathbf{1}\cdot PF_6)_2$[b]	178.7	164.1	3.71	4.71	10.4	90.9

[a] Hydrogen bonds (N1-H1-O12): **1a**: 223, **1b**: 228; $(\mathbf{1}\cdot PF_6)_2$: 230 (N1), and 223 (N1′). [b] Atom numbers with apostrophes.

an isobestic point (Figure 3a). The new band seems to be in accord with the theory of the formation of the π dimer.[4–7] After the solution has stood for some time the color of the probe bleaches out ($\lambda_{max} = 380$ and a shoulder at 351 nm).

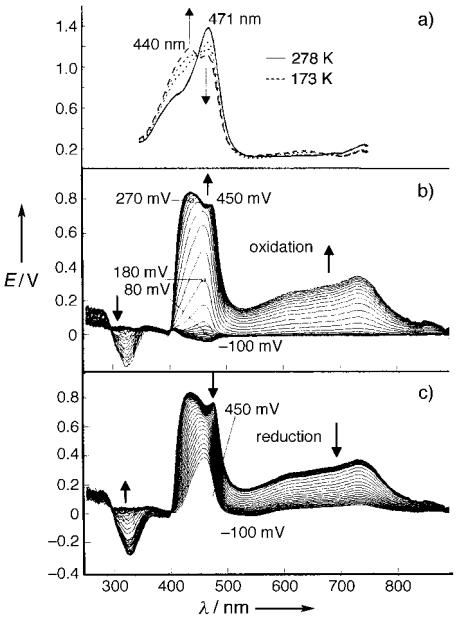

Figure 3. a) UV/Vis spectra of $(\mathbf{1}^{\bullet+}\cdot PF_6)_2$ in CH_2Cl_2 at various temperatures. b) Dependence of the UV/Vis absorption on potential during the oxidation of **1** in the cyclovoltammogram between −100 and 450 mV versus Ag/AgCl. c) Corresponding trace for the reduction. In (a) and (b) the proportion of **1** initially present and of the products that are formed in a photochemical side reaction is substracted.

Low temperature ^1H NMR spectra of $(\mathbf{1}^{\bullet+}\cdot PF_6^-)_2$ in dry and Ar saturated CH_2Cl_2 were obtained in order to identify and characterize the equilibrium component found in the UV/Vis spectrum (Figure 4). At 298 K a spectrum with a very low intensity was found with NH and aromatic protons, as well as four methoxy signals ($\delta = 4.40$, 4.15, 4.08, 3.71) in the ratio 1:5:6 (see spectrum at 273 K). No signals of $\mathbf{1}\cdot^+$ and species in

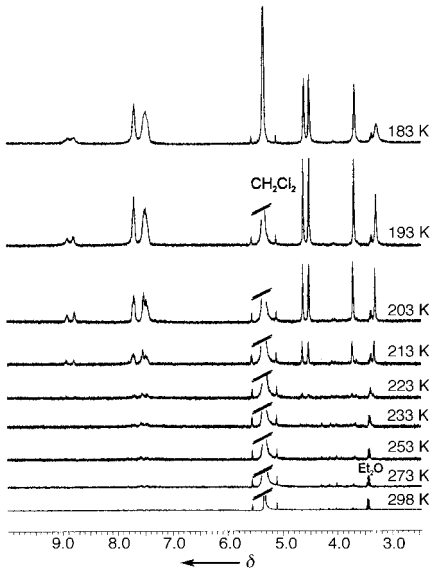

Figure 4. ^1H NMR spectra of a solution of $(\mathbf{1}^{\bullet+}\cdot PF_6)_2$ in CD_2Cl_2 between 298 and 183 K.

equilibrium with it can be observed because of paramagnetic broadening. A new set of proton signals starts to grow out of the background at 223 K and is intensified on further cooling (Figure 4). The intensity can be estimated from the signal corresponding to a trace of diethyl ether.

Surprisingly, the new low temperature spectrum again shows four methoxy signals together with two NH signals and two aromatic multiplets ($\delta =$ 4.61, 4.49, 3.68, 3.28, 7.69, 7.47, 8.90, 8.86; relative intensities 3:3:3:3:2:1:1). Clearly this spectrum is not the one of paramagnetic $\mathbf{1}^{\bullet+}$. On the other hand, one would expect only two methoxy and one NH signals for the π dimer as a result of the free rotation of the methoxy groups in solution. A simultaneous broadening of the the singlets at $\delta = 3.28$ and 8.86 in the spectrum recorded at 183 K shows that such molecular motions just begin to freeze at very low temperature.

In a cyclovoltammetric study of a related thiophene derivative a σ dimerization has been postulated based on

  1433-7851/99/3810-1444 $ 17.50+.50/0 *Angew. Chem. Int. Ed.* **1999**, *38*, No. 10

kinetic and thermodynamic data and a PM3 calculation of the σ dimer.[8b]

Now, in the case of $\mathbf{1}^{\bullet+}$, a σ dimer **9a** or **9b** has for the first time been unequivocally observed by the symmetry of the spinless low temperature species. The π dimer $(\mathbf{1}^{\bullet+}\cdot PF_6^-)_2$ is

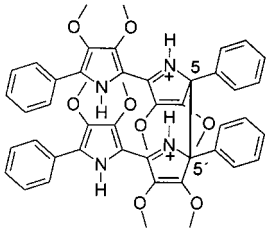

9a

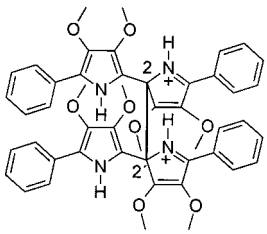

9b

not observed in the low temperature NMR spectrum, it may be present in a very low concentration or in rapid equilibrium with $\mathbf{1}^{\bullet+}$. The fact that only one of eight isomeric σ dimers (including three pairs of enantiomers) is formed may suggest that the C–C bond formation of the radical cations to the σ dimer is preceded by an association step via the π dimer. The observed UV/Vis spectrum (Figure 3a) at low temperature must thus be related to the σ dimer.

After prolonged standing of the solution or addition of traces of water to the probe an NMR spectrum is obtained similar to the 273 K spectrum accompanied by many small signals. The UV/Vis spectrum of this probe is identical to the final spectrum mentioned above. Follow-up reactions of the σ dimer may involve addition of water and partial deprotonation to give several isomers. In the FAB mass spectrum of the solution only the initial radical cation $\mathbf{1}^{\bullet+}$ is seen. Attempts to isolate the modified σ dimer were unsuccessful, only a follow-up product with three methoxy groups was found (EI-MS: $m/z = 390$), which could for example be **10**.

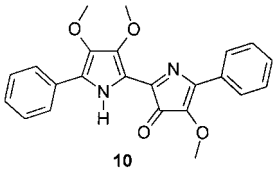

10

The electrochemical oxidation of **1** and the follow-up reactions of $\mathbf{1}^{\bullet+}$ were studied by recording the UV/Vis spectrocyclovoltammograms and simultaneous ESR spectra with a specially designed cell[23] with laminated gold electrodes[24] (Figure 3b, c and 5). The cyclovoltammograms recorded in situ, which were the same as those recorded with conventional disk electrodes, show two reversible waves, only the first of which is shown in Figure 5. The measured ESR intensity is synchronous with the charge flow (Figure 5). The spin concentration n_{ESR} calculated from the calibrated ESR signals shows the concentration of the cation radicals is too low by a factor of about 5 relative to the charge flow for the determined amount of reaction product. The ESR intensity and charge flow vary identically with time, and since a peak current ratio of unity is found in the cyclovoltammogram, the reduced radical concentration cannot arise from an irreversible chemical follow-up reaction. Consequently, there must be a subsequent equilibrium with a spinless dimer.

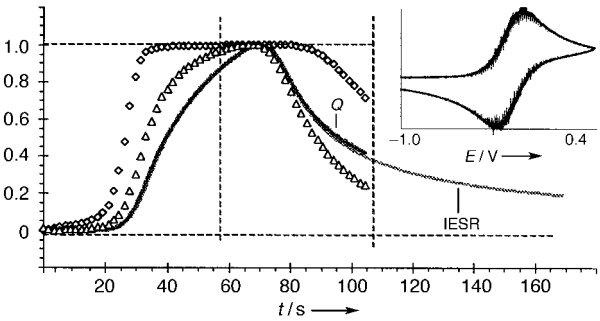

Figure 5. Dependence of the UV/Vis absorptions at 464 (◇) and 735 nm (△), the charge flow Q (black line), and the ESR intensity (grey line) on the potential in the course of a cyclovoltammogram. All four units are normalized with respect to the maximal values. The corresponding CV is shown at the the upper right corner.

The calibrated UV/Vis absorption of $\mathbf{1}^{\bullet+}$ (739 nm) follows the same intensity–time relation as the charge and ESR curves, with the absorption at 464 nm being more complex. In Figures 3a and 3b the formation of two new bands between 400 and 500 nm can be seen. Only at the beginning of the oxidative branch of the cyclovoltammogram is the 464 nm band of $\mathbf{1}^{\bullet+}$ observed, afterwards it is superimposed by the blue-shifted band of the spinless dimer at 430 nm. From the reduction curve (Figure 4c) the chemical and electrochemical reversibility of the entire process is demonstrated.

Experimental Section

1: A solution of **8** (0.578 g, 1 mmol) in Et_2O (2 mL) was added to a solution of Na (0.184 g, 8 mmol) in NH_3. After stirring the solution at −78 °C for 3 h a small amount of aqueous $NaHCO_3$ was added. The NH_3 was removed by a N_2 stream and the residue washed with H_2O (3 × 1 mL). It was then dissolved in CH_2Cl_2 and filtered through Al_2O_3 III. The solvent was removed, and the residue recrystallized from MeOH (0.35 g, 87%) to give needle (**1a**) and cuboid crystals (**1b**, m.p. 171–172 °C). IR (**1a**, KBr): $\tilde{\nu}$ = 3340 cm^{-1} (s, NH); IR (**1b**, KBr): $\tilde{\nu}$ = 3430 cm^{-1} (NH); UV/Vis (CH_3CN): $\lambda(\varepsilon)$ = 371 (32200), 390 (27500) nm; ^1H NMR (250 MHz, $CDCl_3$, basic Al_2O_3): δ = 8.36 (2H, brs, NH), 7.60 (4H, d, J = 7.6 Hz, Ph(H2,H2′)), 7.39 (4H, pseudo-t, J = 7.6 Hz, Ph(H3,H3′)), 7.18 (2H, pseudo-t, J = 7.2 Hz, Ph(H4)), 4.04 (6H, brs" 3,3′-OCH_3), 3.88 (6H, s, 4,4′-OCH_3); ^{13}C NMR (63 MHz, $CDCl_3$, basic Al_2O_3): δ = 137.14 (C4,C4′), 135.05 (C3,C3′), 131.77 (Ph(C1)), 128.85 (Ph(C3,C3′)), 125.51 (Ph(C4)), 123.61 (Ph(C2,C2′)), 115.85 (C5,C5′), 111.39 (C2,C2′), 61.18 (3,3′,4,4′,-OCH_3); EI-MS (70 eV): m/z (%): 404 [$M^{\bullet+}$] (95), 389 [$M-CH_3$]$^+$ (100); FAB-MS (glycerol): m/z (%): 809 [2M+H], (<1), 405 [M+H] (87), 404 [$M^{\bullet+}$] (100), 389 [$M-CH_3^+$] (33).

$(\mathbf{1}\cdot PF_6)_2$: A solution of ferrocinium hexafluorophosphate (33 mg, 0.1 mmol) in CH_3CN (1 mL) was added to **1** (40 mg, 0.1 mmol) in CH_3CN (1 mL) at RT. The resulting green solution was washed with hexanes (3 × 5 mL) to remove excess ferrocene and kept for 48 h at −20 °C under exclusion of light and moisture. This produced $(\mathbf{1}\cdot PF_6)_2$ (40 mg, 72%) as bluish-black needles, which above 250 °C decompose without melting. IR: $\tilde{\nu}$ = 3430 (NH), 2995, 2938, 2854, 1544, 1372, 1013, 830 (PF), 777, 688, 558 cm^{-1}; MS (FAB, CH_2Cl_2/nitrobenzyl alcohol matrix): m/z: 404 [$\mathbf{1}^{\bullet+}$]

The preparation of precursors **1-8** is given in the supporting information.

Received: October 12, 1998
Revised version: February 19, 1999 [Z12518IE]
German version: *Angew. Chem.* **1999**, *111*, 1533–1538

Keywords: cyclic voltammetry · dimerizations · oligomers · pyrrole · radical ions

  1433-7851/99/3810-1445 $ 17.50+.50/0

[1] a) A. Merz, R. Schropp, *Adv. Mater*. **1992**, *4*, 409 – 411. b) A. Merz, R. Schropp, J. Lex, *Angew. Chem.* **1993**, *105*, 296 – 298; *Angew. Chem. Int. Ed. Engl.* **1993**, *32*, 291 – 293. c) A. Merz, R. Schropp, E. Dötterl, *Synthesis* **1995**, 795 – 800.
[2] a) A. Merz, S. Graf, *J. Electroanal. Chem.* **1996**, *412*, 11 – 17; b) F. Gassner, S. Graf, A. Merz, *Synth. Met.* **1997**, *87*, 75 – 79.
[3] M. Amleida, R. T. Henriques in *Handbook of Organic Conductive Molecules and Polymers* (Ed:. H. S. Nalwa), Wiley, Chichester, **1997**, pp. 87 – 150; G. C. Papavassiliou, A. Terzis, P. Delhaes Henriques in *Handbook of Organic Conductive Molecules and Polymers* (Ed.: H. S. Nalwa), Wiley, Chichester, **1997**, pp. 151 – 227.
[4] J. A. E. H. van Haare, L. Groenendahl, E. E. Havinga, R. A. J. Janssen, E. W. Meijer, *Angew. Chem*. **1996**, *108*, 696 – 699; *Angew. Chem. Int. Ed. Engl*. **1996**, *35*, 638 – 640.
[5] a) P. Bäuerle, U. Segelbacher, K.-U. Gaudl, D. Huttenlocher, M. Mehring, *Angew. Chem*. **1993**, 105, 125 – 127; *Angew. Chem. Int. Ed. Engl*. **1993**, *32*, 76 – 78; a) P. Bäuerle, U. Segelbacher, A. Maier, M. Mehring, *J. Am. Chem. Soc*. **1993**, *115*, 10217 – 10223.
[6] a) L. L. Miller, Y. Yu, E. Gunic, R. Duan, *Adv. Mater.* **1995**, *7*, 547 – 548; b) Y. Yu, E. Gunic, B. Zinger, L. L. Miller, *J. Am. Chem. Soc*. **1996**, *118*, 1013 – 1018
[7] M. P. Cava, J. P. Parakka, J. A. Jeevarajan, A. S., Jeevarajan, L.D. Kispert, *Adv. Mater.* **1996**, *8*, 54 – 59.
[8] a) A. Smie, J. Heinze, *Angew. Chem*. **1997**, *109*, 375 – 379; *Angew. Chem. Int. Ed. Engl.* **1997**, *36*, 363 – 367. b) P. Tschunky, J. Heinze, A. Smie, G. Engelmann, G. Kossmehl, *J. Electroanal. Chem.* **1997**, *433*, 223 – 226.
[9] D. D. Graf, R. G. Duan, J. P. Campbell, L. L. Miller, K. R. Mann, *J. Am. Chem. Soc*. **1997**, *119*, 5888 – 5899.
[10] P. G. Gassman, W. N. Schenk, *J. Org. Chem*. **1977**, *42*, 918 – 920.
[11] R. Chong, P. S. Clezy, *Aust. J. Chem*. **1967**, *20*, 935 – 950.
[12] D. Peters, A.-B. Hörnfeldt, S. Gronowitz, *J. Heterocycl. Chem*. **1991**, *28*, 526 – 531.
[14] S. Baroni, R. Stradi, *J. Heterocycl. Chem*. **1980**, *17*, 1221.
[15] J. Kronberger, unpublished results.
[16] Crystal sructures: **1a** (tetragonal isomorph)**:** $C_{24}H_{24}N_2O_4$, $M_r = 404.47$, yellow crystals from MeOH, m.p. 171 – 172 °C; crystal dimensions: $0.50 \times 0.13 \times 0.13$ mm; tetragonal, space group $I4_1cd$ (No. 110), $a = 18.831(3)$, $b = 18.831(3)$, $c = 11.639(2)$ Å, $\alpha = 90°$, V = 4127.3(12) Å^3, $Z = 8$, $\rho_{calcd} = 1.302$ g cm^{-3}; $F(000) = 1712$; $\mu_{Cu} = 7.3$ cm^{-1}; $\theta_{max} = 74.97°$; 4372 determined, 2058 independent, 1918 observed reflexions with ($F_o^2 > 2\sigma F_o^2$); $R1 = 0.0260$, $wR2 = 0.0714$, GOF (F^2) = 1.083 for 137 parameters, residual electron density 0.026/ – 0.092 e Å^{-3}. **1b** (monoclinic isomorph): $C_{24}H_{24}N_2O_4$, $M_r = 404.47$, yellow crystals from MeOH, m.p. 171 – 172 °C; crystal dimensions: $0.20 \times 0.20 \times 0.09$ mm; monoclinic, space group $P2_1/n$ (No. 14), $a = 7.943(1)$, $b = 10.499(1)$, $c = 12.7930(1)$ Å, $\alpha = 90$, $\beta = 107.00(1)°$, V = 1020.24(19) Å^3, $Z = 2$, $\rho_{calcd} = 1.317$ g cm^{-3}; $F(000) = 428$; $\mu_{Cu} = 7.3$ cm^{-1}; $\theta_{max} = 75°$; 2200 determined, 2017 independent, 1662 observed reflections ($F_o^2 > 2\sigma F_o^2$); $R1 = 0.0358$, $wR2 = 0.1183$, GOF (F^2) = 1.004 for 139 parameters, residual electron density 0.215/ – 0.132 e Å^{-3}. $(\mathbf{1} \cdot PF_6)_2$: $(C_{24}H_{24}N_2O_4F_6P)_2$, $M/2 = 549.43$, bluish-black needles, decomp. > 250 °C; crystal dimensions: $0.25 \times 0.08 \times 0.03$ mm; triclinic, space group $P\bar{1}$ (No. 2), $a = 8.36(1)$, $b = 11.220(1)$, $c = 13.067(1)$ Å, $\alpha = 111.78(1)$, $\beta = 96.23(1)$, $\gamma = 90.56(1)°$; $V = 1129.8(8)$ Å^3, $Z = 2$, $\rho_{calcd} = 1.444$ g cm^{-3}; $F(000) = 510$; $\mu_{Mo} = 1.021$ cm^{-1}; $\theta_{max} = 59.99$; 3304 determined 3304 independent, 1813 observed refections ($F_o^2 > 2\sigma F_o^2$); $R1 = 0.0496$, $wR2 = 0.1234$, GOF (F^2) = 0.908 for 339 parameters, residual electron density 0.297/ – 0.216 e Å^{-3}. The crystallographic data (excludung structure factors for the structures reported in this paper have been deposited with the Crystallographic Data Centre as supplementary publication nos CCDC-102195 (**1a**), -102194 (**1b**), and -102196 $(\mathbf{1} \times PF_6)_2$. Copies of the data can be obtained free of charge on application to CCDC, 12 Union Road, Cambridge CB21EZ, UK (fax: (+44) 1223-336-033; e-mail deposit@ccdc.cam.ac.uk).
[17] H. J.Keller, D. Nöthe, H. Pritzkow, D. Wehe, M. Werner, P. Koch, D. Schweitzer, *Mol. Cryst. Liq. Cryst*. **1980**, *62*, 181 – 199.
[18] N. Thorup, G. Rindorf, H. Soling, K. Bechgard, *Acta Crystallogr. Ser. B* **1981**, *37*, 1236 – 1250.
[19] J. Fuhrhop, P.Wasser, D. Riesner, D. Mauzerall, *J. Am. Chem. Soc*. **1972**, **94**, 1996 – 8001.
[20] K. Kimura, T. Yamazaki, S. Katsumata, *J. Phys. Chem.* **1971**, *75*, 1768 – 1774.
[21] W. Geuder, S. Hünig, *Tetrahedron* **1986**, *42*, 1665 – 1677.
[22] A. Bondi, *J. Chem. Phys.***1964**, *68*, 441 – 445.
[23] A. Petr, L. Dunsch, A. Neudeck, *J. Electroanal. Chem.* **1996**, *412*, 153 – 158.
[24] A. Neudeck, L. Kress, *J. Electroanal. Chem.* **1998**, *437*, 141 – 156.

Topological Links between Duplex DNA and a Circular DNA Single Strand**

Heiko Kuhn,* Vadim V. Demidov,* and Maxim D. Frank-Kamenetskii*

DNA is well known to adopt various topological (and pseudotopological) structures like knots, catenanes, Borromean rings, and pseudorotaxanes.[1] It has long been recognized that DNA topology plays a crucial role in such fundamental biological phenomena as DNA supercoiling and topoisomerization.[2] Another reason for the considerable interest in higher order DNA topology structures stems from the realization that DNA topological and pseudotopological forms may provide stable and sequence-specific targeting of DNA. Accordingly, highly localized DNA detection and precise spatial positioning of various ligands on the DNA scaffold become possible. This may lead to new applications in molecular biotechnology, in gene therapy, and in the emerging field of DNA nanotechnology.[1d, 3]

In this connection, one of the promising DNA pseudotopological constructions is the DNA padlock, consisting of a long single-stranded (ss) DNA molecule forming a pseudorotaxane with a short cyclic oligodeoxyribonucleotide (cODN).[4] Another interesting pseudorotaxane-type structure, the sliding clamp, contains a short cODN threaded on double-stranded (ds) DNA.[1c] Notwithstanding the value of the indicated pseudotopological structures for DNA labeling, note that in these constructions the cODN tag is allowed to slide along the target for considerable distances, compromising the precision of spatial positioning of the label.

We have assembled a new supramolecular structure, a linked DNA pseudorotaxane, in which part of a cODN appears to be threaded sequence specifically between complementary strands of dsDNA (see Scheme 1 and Figure 1 a). Our structure forms a true topological link as long as the

[*] Dr. H. Kuhn, Dr. V. V. Demidov, Prof. M. D. Frank-Kamenetskii
Center for Advanced Biotechnology
and Department of Biomedical Engineering
Boston University
36 Cummington Street, Boston, MA 02215 (USA)
Fax: (+1) 617-353-8501
E-mail: hkuhn@bu.edu
vvd@enga.bu.edu
mfk@enga.bu.edu

[**] Support by the National Institutes of Health and PerSeptive Biosystems (now PE Biosystems) is appreciated. We thank Dr. M. Egholm and Dr. P. E. Nielsen for providing us with PNA oligomers.

  1433-7851/99/3810-1446 $ 17.50+.50/0